JAST, 2018;11(2):49-58

2-DIMENSIONAL STRAIGHT-LINE PATH FOLLOWING AND SIMULATION OF AN UNMANNED AERIAL VEHICLE

Zafer ÖZNALBANT* **Uğur ÖZDEMİR** **Mehmet Şerif KAVSAOĞLU**

Turkish Aerospace Industries
Ankara, Türkiye,
zafer.oznalbant@tai.com.tr

Anadolu University, Faculty of Aeronautics and Astronautics
Eskişehir, Türkiye
ugurozdemir@anadolu.edu.tr

Anadolu University, Faculty of Aeronautics and Astronautics
Eskişehir, Türkiye
mskavsaoglu@anadolu.edu.tr

Received: *27th February 2018* ***Accepted:*** *06th June 2018*

ABSTRACT

In this paper, a two-dimensional-straight-line path following methodology for an unmanned aircraft is developed. With the developed algorithm, the unmanned aerial vehicle is made to converge to a predefined path, and then to follow a virtual target on the path. Unlike similar algorithms, the location of virtual target is defined as a function of the distance between the aircraft and path itself. By this way, according to the distance between the aircraft and path, the aircraft firstly heads directly to the path then follow it to the next point. The location of the virtual target is changed according to the magnitude of the cross track error which is the distance between the path and the aircraft itself. After defining the equations required for the calculation of the desired heading, the applied closed controller is explained. A numerical simulation model is created for the solution of equations of motion to investigate the outputs of the path following algorithm. The results of the algorithm and simulation are evaluated.

Keywords: *Unmanned Aerial Vehicle, Path Following, Numerical Simulation.*

İNSANSIZ HAVA ARACININ 2 BOYUTLU ÇİZGİSEL YÖRÜNGE TAKİBİ VE SİMÜLASYONU

ÖZET

Bu çalışmada, insansız bir uçak için iki boyutlu çizgisel yörünge takip yöntemi geliştirilmiştir. Benzer algoritmalardan farklı olarak, sanal hedefin konumu uçak ve yörünge arasındaki mesafenin bir fonksiyonu olarak tanımlanmıştır. Bu sayede, uçak ile yörünge arasındaki mesafeye göre uçak öncelikle yörüngeye doğru yönelir ve ardından bir sonraki noktaya kadar yörüngeyi takip eder. Sanal hedef noktasının yörünge üzerindeki konumu, uçak ile yörünge arasındaki uzaklık olarak tanımlanan sapma hatasının büyüklüğüne göre değiştirilmiştir. İstenilen istikamet açısının hesaplanması için kullanılan denklemler tanımlandıktan sonra, kullanılan kapalı çevrim kontrolör kısaca tanıtılmıştır. Yörünge takibi algoritması çıktılarının incelenebilmesi için hareket denklemlerinin sayısal yöntemlerle çözüldüğü benzetim uygulaması yapılmıştır. Yörünge takip algoritması ve benzetim sonuçları değerlendirilmiştir.

Anahtar Kelimeler: *İnsansız Hava Aracı, Yörünge Takibi, Sayısal Benzetim (Simülasyon).*

1. INTRODUCTION

Path and trajectory following algorithms or control methods experience an increase in popularity with the increasing demand for UAVs. The difference between the path following and the trajectory following is the time parameter. In the trajectory following, the vehicle is required to be in a predefined position at the predefined time. In the path following, the vehicle is required to be in a position independent of time. The path following algorithm is a combination of control law(s) and required algorithm which command the vehicle to follow a predefined two or three-dimensional straight or orbital path. The aim of

* Corresponding Author

the path following algorithms for unmanned aircraft is first to calculate the cross track error and then calculate the desired heading command which eventually makes the cross track error zero. The desired heading command is required to send to the aircraft low-level autopilot or directly to the actuators in order to make the aircraft follow the path.

In the literature, there are several path following algorithms according to their computational methods [1-5, 7]. These methods can be categorized as direct waypoint (WP) heading algorithms, virtual target (VT) heading algorithms, and the vector field based path following algorithms [1]. The direct waypoint algorithms do not deal with the path itself. The main idea of this kind of algorithms is to calculate the vehicle position according to the next waypoint and head the vehicle directly to the waypoint. In the virtual target heading algorithms, there assumed a virtual target on the path and the algorithm aims to chase this virtual target [2]. This kind of path following algorithms is also called carrot-chasing or rabbit-chasing algorithms. The objective of the vector field based algorithms is also to calculate or select a heading angle so that the cross track error is driven to zero. The idea behind the vector field strategy is to construct a field of which every point defines the desired heading angle toward the straight path [3]. Dubins path is another path following strategy in which, the time-optimal path is defined between two configurations. Each configuration consists of a position and a heading [4]. In this strategy, a path is established with differential constraints according to the methods given in the Dubin's paper in 1957. In this method, the airplane is assumed to be steering only by rudder displacements [4, 5].

In several sources, the course angle is also defined. The difference between the course and the heading angle is that the course angle defines the direction of movement in wind. On the other hand, the heading angle defines the aircraft nose direction. If the winds are assumed to have zero velocity, and there is not any rudder deflection to change the heading, the course angle, and the heading angle can be assumed to be the same.

After calculating or selecting the heading angle which eventually makes the cross track error zero, a kind of control method must be considered to make the aircraft follow the desired heading. It can be performed by several methods [6]. One of them can be using the rudder deflection to lean the aircraft toward the desired heading. Because of the couplings and the aerodynamic efficiency, this method is not a convenient way for a maneuvering flight. The second and a more convenient method for maneuvering flight is the coordinated turn [7]. The coordinated turn can be explained as a constant altitude turn with a bank angle (ϕ). During the coordinated turn, the centripetal forces are balanced by the lift vector component [8]. There is the last point to be considered that what kind of controller or guidance law to be used to calculate the signals for actuators. These can be Linear quadratic regulator (LQR), backstepping or proportional/integral/derivative (PID) controllers.

In this study, a two-dimensional straight-line path following problem is analyzed. Although, a classical VT approach has been selected as a baseline, the study is distinguished from similar methodologies by defining a variable VT location according to the aircraft position. More clearly, the virtual target location on the path is defined as a function of the aircraft position, and the VT moves forward while the aircraft approaches to the path. By this way, instead of directly heading to the VT, the aircraft firstly converges to a predefined straight path line and then follows this line to the next waypoint.

At the very beginning of the simulation, the aircraft has been forced to approach to the closest point on the path according to the distance between the path and aircraft itself, then forced to follow the path to the next waypoint as the cross track error becomes smaller. With the developed simulation, the position, states and the control surface displacements of the aircraft have been recorded. The aerodynamic and propulsion model of the aircraft investigated in this paper have been gathered from Aerosonde UAV given in reference [9]. It is also assumed that the wind velocity is zero. In the following sections; the problem definition and the solution method are given, the numerical simulation technique is described, and the simulation results are summarized.

2. PROBLEM DEFINITION AND THE SOLUTION METHOD

2.1. Problem Definition

At the beginning of the simulation, the aircraft is located arbitrarily near a 2D path line. According to the scenario, the aircraft is desired to fly toward the path first then follow the path to the next WP while it is approaching the path. The aircraft location and straight-line path is depicted in Fig. 1. In Fig. 1, AC defines the aircraft, and the dashed red line defines the

path to be followed. The cross track error (e_{ct}) is the closest distance between the vehicle and the path. The closest point (CP) is the intersection between the path and the cross track error line. The objective is to design a path following method by which the aircraft firstly fly towards the path itself according to the magnitude of e_{ct} and as it approaches to the path, it maneuvers to fly tangent to the path toward the next WP. Eventually, it is desired to eliminate the cross track error and heading to the next WP.

2.2. Solution Method

For the solution method, a virtual target-chasing algorithm with a proportional compensated closed loop algorithm is used. First, the closest point location on the path is defined as;

$$|\boldsymbol{r}| = \|\boldsymbol{AC} - \boldsymbol{WP_i}\| \tag{1}$$

$$\boldsymbol{\varepsilon} = \tan^{-1}\left(\frac{y-y_i}{x-x_i}\right) \tag{2}$$

$$\boldsymbol{e_{ct}} = |\boldsymbol{r sin\varepsilon}| \tag{3}$$

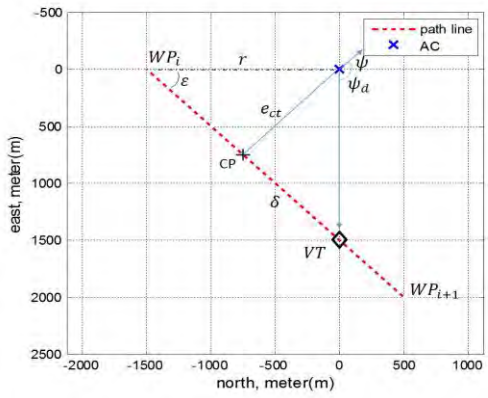

Figure 1. The 2D position of an aircraft relative to the straight line path. AC (x,y): aircraft position; WPi (x_i+y_i): previous waypoint; WP_{i+1} (x_i+y_i): Next waypoint; VT (x_t+y_t): virtual target point, ect:cross track error, ψ:current heading of the aircraft, ψ_d:desired heading; ε: azimuth angle between the aircraft and path line; δ: the distance between virtual target point and closest point; CP: closest point location on the path.

After calculating the closest point location on the path the cross track error which is the perpendicular distance between the aircraft and the path is calculated. Then, the virtual target point is defined on the path. Equation (1) presents the distance between the aircraft and the first waypoint. Equation (2) presents the azimuth angle of aircraft and Eqn. (3) presents the cross track error. The position of the virtual target is parametrized with the cross track error and given in Eqn. (4). Therefore, according to the cross track error magnitude, the virtual target distance from the closest point changes simultaneously. For the large value of cross track error, the virtual target point is getting closer to the closest point on the path. On the other hand, while the aircraft is getting closer to the closest point, the virtual target is getting further from the closest point and heading to the next WP. For this study, the maximum virtual target distance from the closest point is assigned as 300 meters, and it is coded if the cross track error greater than 300 meters, the aircraft is commanded to fly directly to the closest point. This methodology makes the aircraft catch the path quicker than a constant virtual target distance case. The desired heading angle is defined as the line between the aircraft and the virtual target point on the path.

The distance between the closest point and virtual target is calculated as;

$$\boldsymbol{\delta e_{ct}} = \begin{cases} \boldsymbol{0} & \boldsymbol{|e_{ct}| \le 300} \\ \boldsymbol{300 - |e_{ct}|} & \boldsymbol{|e_{ct}| < 300} \end{cases} \tag{4}$$

The desired heading angle is calculated as;

$$\boldsymbol{\psi_d} = \tan^{-1}\left(\frac{y-y_t}{x-x_t}\right) \tag{5}$$

After calculating the desired heading angle, the closed loop controller given in Fig. 2 is used to control the airplane properly. In Fig. 2, the block named 'Coordinated Turn Coupling Function' is the block in which the required reference heading is calculated according to the position of the virtual target. The reference bank angle is defined as a predetermined ratio between the actual heading angle and the reference heading angle. According to the defined bank angle and the true airspeed of the airplane, the reference yaw rate (R_d) and pitch rate (Q_d) are calculated with the help of coordinated turn relations [10]. (R_d) and pitch rate (Q_d) equations are given in Eqn. (6) and (7), respectively.

$$\boldsymbol{R_d} = \frac{\boldsymbol{g \sin\phi}}{\sqrt{\boldsymbol{U^2+V^2+W^2}}} \tag{6}$$

$$\boldsymbol{Q_d} = \boldsymbol{R_d \tan\phi} \tag{7}$$

In Fig. 2, the output of 'Aircraft Dynamics' block diagram represents 12 states which are the position, attitude, linear velocities, and angular rates of the aircraft.

The aileron, rudder, and elevator actuator blocks in Fig. 2 consists of first order lag transfer function with 0,1 second time constant.

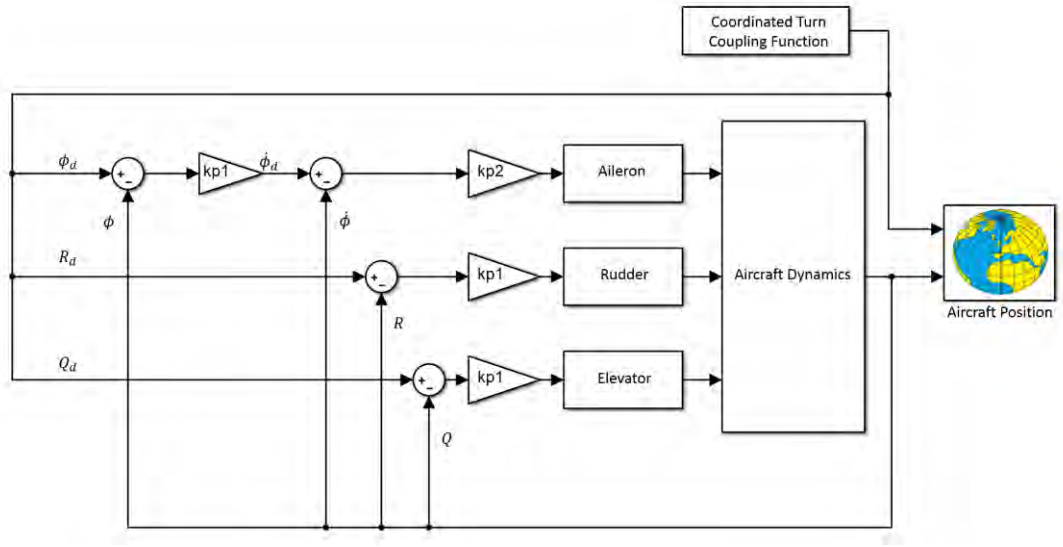

Figure 2. The nested closed loop controller for coordinated turn in order to get the reference heading. ψ_d is the reference heading; ϕ_d is the reference bank angle for the coordinated turn; k_{p1} and k_{p2} are gains of the outer and inner loop, respectively.

3. NUMERICAL SIMULATION METHOD

A numerical calculation based simulation is prepared to analyze the aircraft responses. The general equations of motions are modeled in the MATLAB Simulink software. Twelve ordinary differential equations, which describe the aircraft motion, are modeled [8, 11, 12] and given in Eqns. (8) – (19).

$$\begin{aligned}\dot{x_E} = {} & U\cos\theta\cos\psi \\ & + V(\sin\phi\sin\theta\cos\psi \\ & - \cos\phi\sin\psi) \\ & + W(\cos\phi\sin\theta\cos\psi \\ & + \sin\phi\sin\psi)\end{aligned} \tag{8}$$

$$\begin{aligned}\dot{y_E} = {} & U\cos\theta\sin\psi \\ & + V(\sin\phi\sin\theta\sin\psi \\ & + \cos\phi\cos\psi) \\ & + W(\cos\phi\sin\theta\sin\psi \\ & - \sin\phi\cos\psi)\end{aligned} \tag{9}$$

$$\begin{aligned}\dot{z_E} = {} & -U\sin\theta + V\sin\phi\cos\theta \\ & + W\cos\phi\cos\theta\end{aligned} \tag{10}$$

$$\dot{u} = -QW + RW + \frac{1}{m}F_x \tag{11}$$

$$\dot{v} = -ru + pw + \frac{1}{m}F_y \tag{12}$$

$$\dot{w} = -pv + qu + \frac{1}{m}F_z \tag{13}$$

$$\dot{\phi} = P + Q\sin\phi\tan\theta + R\cos\phi\cos\theta\tan\theta \tag{14}$$

$$\dot{\theta} = Q\cos\phi - R\sin\phi \tag{15}$$

$$\dot{\psi} = (R\cos\phi + Q\sin\phi)/\cos\theta \tag{16}$$

$$\dot{P} = \frac{\Gamma_4 + \Gamma_6\frac{I_{xz}}{I_{xx}}}{1 - \frac{I_{xz}^2}{I_{xx}I_{zz}}} \tag{17}$$

$$\dot{Q} = \frac{1}{I_{yy}}(PR(I_{zz} - I_{xx}) - (P^2 - R^2)I_{xz} + M) \tag{18}$$

$$\dot{R} = \frac{\Gamma_6 + \Gamma_4\frac{I_{xz}}{I_{xx}}}{1 - \frac{I_{xz}^2}{I_{xx}I_{zz}}} \tag{19}$$

The Γ_4 and Γ_6 are given in (20) and (21), respectively.

$$\Gamma_4 = \frac{1}{I_{xx}}\left(-QR\left(I_{zz} - I_{yy}\right) + \left(\dot{R} + PQ\right)I_{xz} + L\right) \tag{20}$$

$$\Gamma_6 = \frac{1}{I_{zz}}\left(-PQ\left(I_{yy} - I_{xx}\right) - \left(QR - \dot{P}\right)I_{xz} + N\right) \tag{21}$$

One of the modeled equation in Simulink® is given in Fig. 3. In Fig. 3, the $\dot{u}$ equation, given in Eqn. (11), is presented. The function which is given in Eqn. (11) is typed into the f(u) block in the model. After starting the simulation, the equations are solved by the embedded numerical solution method Runge-Kutta with a fixed step size. The Simulink® software is chosen because of the visualization capabilities and user-friendly interface. These equations can also be solved with a prepared numerical solution code such as 4th order Runge-Kutta or Euler methods.

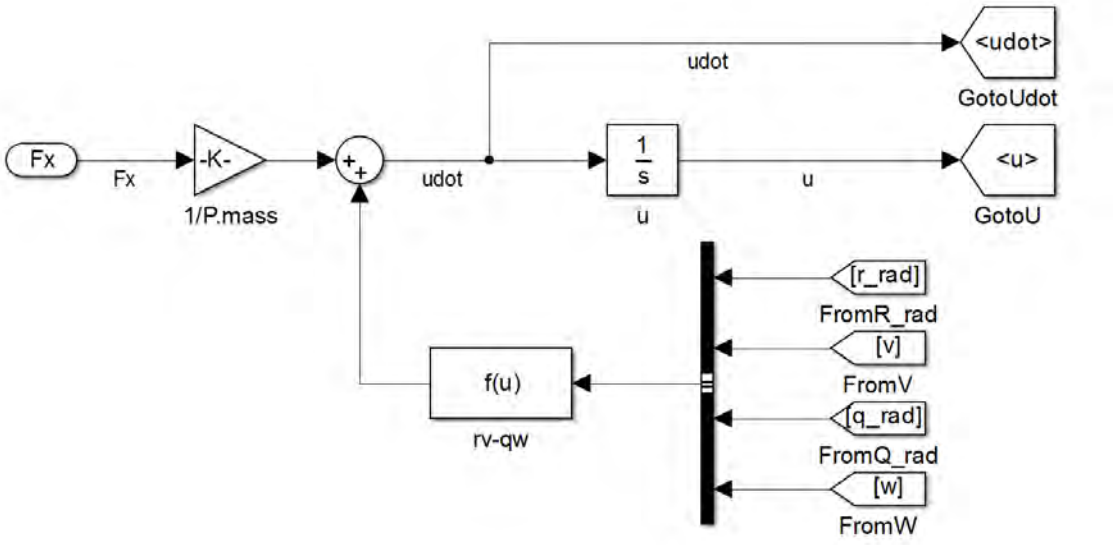

Figure 3. The $\dot{u}$ equation modelling Simulink.

F_x, F_y, F_z and L, M, N terms are the components of the external forces and moments acting on the aircraft in x-, y-, and z-axis respectively. The force and moment terms required in Eqn. (8)-(21) are also calculated with another block modeled in Simulink. The equations for calculating the aerodynamic forces and moments are gathered from the Ref. [9] and given in Eqn. (22)-(39).

$$C_L = C_{L_0} + C_{L_\alpha}\alpha \tag{22}$$

$$C_D = C_{D_0} + C_{D_\alpha}\alpha \tag{23}$$

$$C_m = C_{m_0} + C_{m_\alpha}\alpha + C_{m_q}\frac{q\bar{c}}{2V} + C_{m_{\delta_e}}\delta_e \tag{24}$$

$$C_Y = C_{L_0} + C_{L_\beta}\beta + C_{Y_p}\frac{pb}{2V} + C_{Y_r}\frac{rb}{2V} + C_{Y_{\delta_r}}\delta_r \tag{25}$$

$$C_l = C_{l_0} + C_{l_\beta}\beta + C_{l_p}\frac{pb}{2V} + C_{l_r}\frac{rb}{2V} + C_{l_{\delta_a}}\delta_a + C_{l_{\delta_r}}\delta_r \tag{26}$$

$$C_n = C_{n_0} + C_{n_\beta}\beta + C_{n_p}\frac{pb}{2V} + C_{l_r}\frac{rb}{2V} + C_{l_{\delta_a}}\delta_a + C_{l_{\delta_r}}\delta_r \tag{27}$$

$$C_{x_a} = -C_D\cos\alpha + C_L\sin\alpha \tag{28}$$

$$C_{x_q} = -C_{D_q}cos\alpha + C_{L_q}sin\alpha \tag{29}$$

$$C_{x_{\delta e}} = C_{D_{\delta e}}cos\alpha + C_{L_{\delta e}}sin\alpha \tag{30}$$

$$C_{z_a} = -C_D sin\alpha - C_L cos\alpha \tag{31}$$

$$C_{z_q} = -C_{D_q} sin\alpha - C_{L_q} cos\alpha \tag{32}$$

$$C_{z_{\delta e}} = -C_{D_{\delta e}} sin\alpha - C_{L_{\delta e}} cos\alpha \tag{33}$$

$$F_{X_A} = Q_{dyn}S_{ref}\left(C_{x_a} + C_{x_q}\frac{q\bar{c}}{2V} + C_{x_{\delta e}}\delta_e\right) \tag{34}$$

$$F_{Y_A} = Q_{dyn}S_{ref}C_Y \tag{35}$$

$$F_{Z_A} = Q_{dyn}S_{ref}\left(C_{z_a} + C_{z_q}\frac{q\bar{c}}{2V} + C_{z_{\delta e}}\delta_e\right) \tag{36}$$

$$L_A = Q_{dyn}S_{ref}C_l b \tag{37}$$

$$M_A = Q_{dyn}S_{ref}C_m\bar{c} \tag{38}$$

$$N_A = Q_{dyn}S_{ref}C_n b \tag{39}$$

Gravitational forces are given in Eqn. (40)-(42).

$$F_{X_G} = -\mathrm{W}\sin\theta \tag{40}$$

$$F_{Y_G} = \mathrm{W}\cos\theta\sin\phi \tag{41}$$

$$F_{Z_G} = \mathrm{W}\cos\theta\cos\phi \tag{42}$$

It has been assumed that there is no any propulsion induced moment and the thrust induced by propeller is constant.

For the simulation initial conditions, the cruise trim parameters for the aircraft given in the reference [9] have been used.

For the coordinated turn approximation, the thrust ratio also must be auto controlled in order to sustain the sufficient the lift increment, airspeed, and altitude implicitly. In this study, the thrust ratio remains as a constant value. Besides, after the simulation has finished, it was seen that the altitude and the velocity had a smooth change during the simulation.

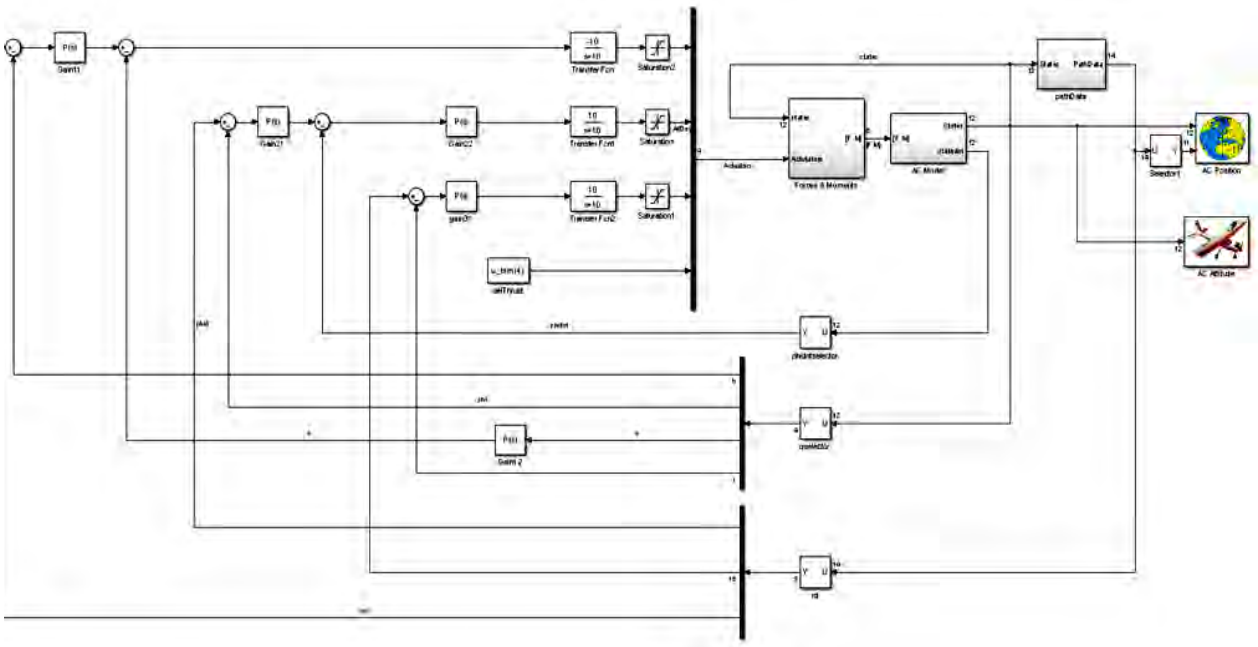

Figure 4. The whole model created in Simulink in order to simulate the aircraft motion.

4. SIMULATION RESULTS

4.1. Path Following Results

Fig. 5 is depicting the completed path following simulation performed by the aircraft and a visual capture from airplane attitude investigation. At the beginning of the simulation, the aircraft positioned at the origin (0, 0) with the initial heading to the positive x-axis (north). In Fig. 5, the dashed (red) line shows the predefined path which is desired to be followed by the aircraft. The solid (blue) line shows the flight path performed by the aircraft during the simulation. The diamond shape is indicating the virtual target position on the path, and the cross is indicating the closest point between the aircraft and predefined path. The time process of the path generation is given in Fig. 6. In Fig. 6, the path followed by the aircraft, the closest point on the path and the virtual target locations are given for 10^{th}, 20^{th}, 40^{th}, and 80^{th} seconds of the simulation. It can be seen from the figure that the virtual target point is matching with the closest point on the path since the cross track is greater than the predefined value. Therefore, the aircraft is heading directly to the closest point at the 10^{th} second. While the aircraft is getting closer to the path, the cross track error becomes smaller and the virtual target starts to separate from the closest point and moves toward the next waypoint direction. This separation can be seen in 20^{th} second in Fig. 6. As the aircraft gets closer to the path itself, the virtual target moved farther from the closest point. By this way, the aircraft flies smoothly toward the virtual target and starts to follow through the path. At the 80^{th} second, since the cross track error has the smallest value, the virtual target is placed most forward position toward the next waypoint. Since the desired heading is calculated according to the virtual target point, the aircraft heads to the virtual target and eventually the cross track error goes to zero.

4.2. The Changes of States According to the Simulation Time

The control surface deflections, the linear and angular velocities of the aircraft, position and attitude were calculated to determine the maneuvers made by the aircraft while the simulation was running. The reference heading angle, measured heading angle, reference yaw angle, measured yaw angle, and deviation in cross track error recorded during the simulation are shown in Fig 7. As shown in Fig. 7, when the cross track error is large, the airplane is flying directly toward the path itself, starting to turn at a high angle of roll. As the cross track error decreases, the virtual target moves away from the projection point. Depending on the position of the virtual target,

the direction of the heading changes. When the cross track error approaches zero, the plane approaches the path line by rolling and follows the virtual target point. Fig. 8 shows the variation of the aileron, rudder, and elevator displacements are recorded during the simulation according to the cross track error. The time-dependent variation of 12 state variables of the aircraft during this period is shown in Fig 9.

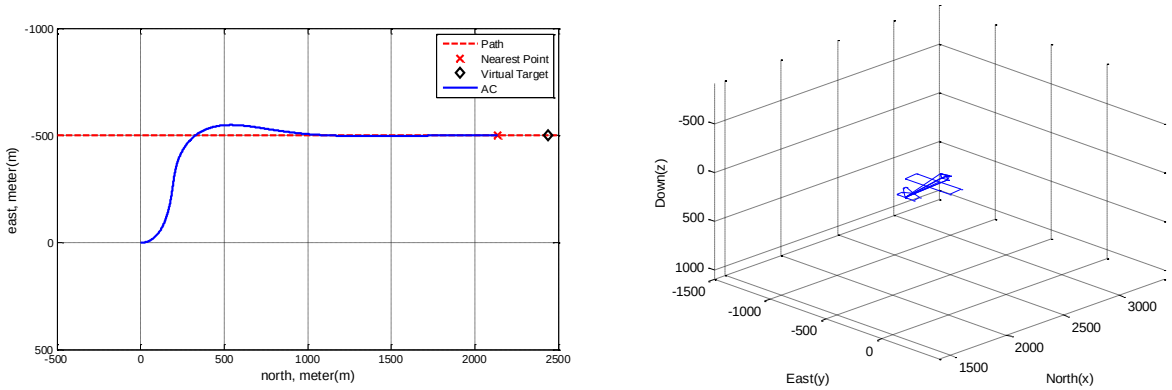

(a) (b)

Figure 5. a) The path followed by the aircraft which was headed to the moving virtual target. b) aiplane attitude visualisation during simulation.

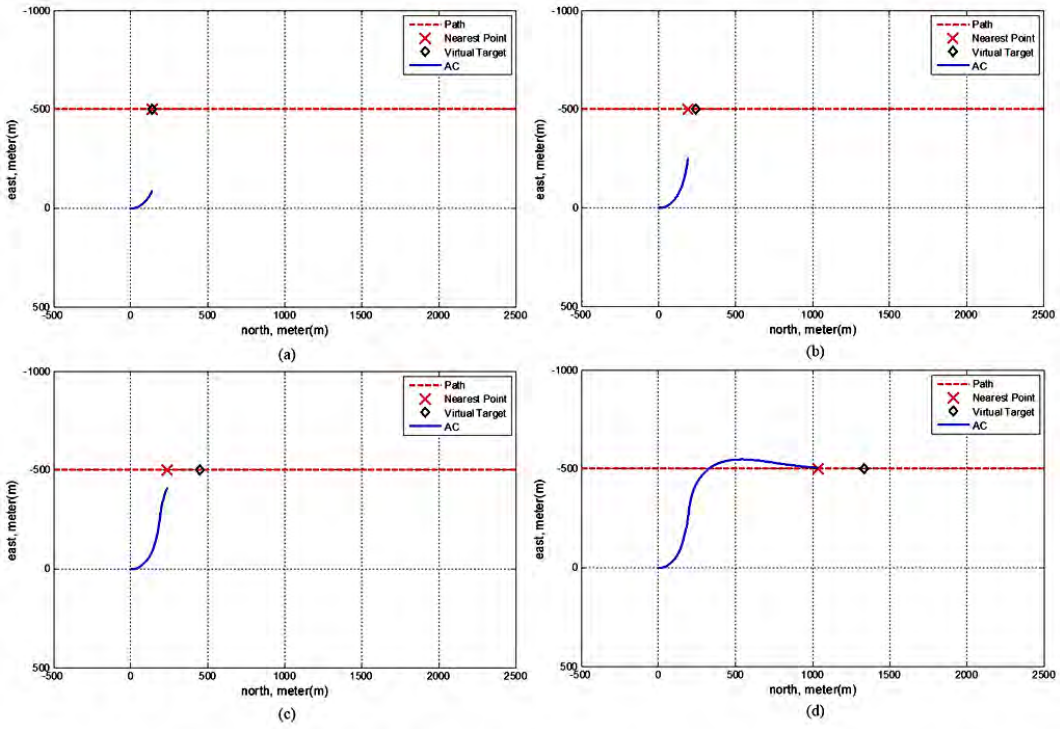

Figure 6. The positions of the aircraft (AC), Virtual Target, and the Closest Point according to time progress. (a) is presenting the positions for 10th second, (b) is presenting the positions for 20th second, (c) is presenting the positions for 40th second, (d) is presenting the positions for 80th second.

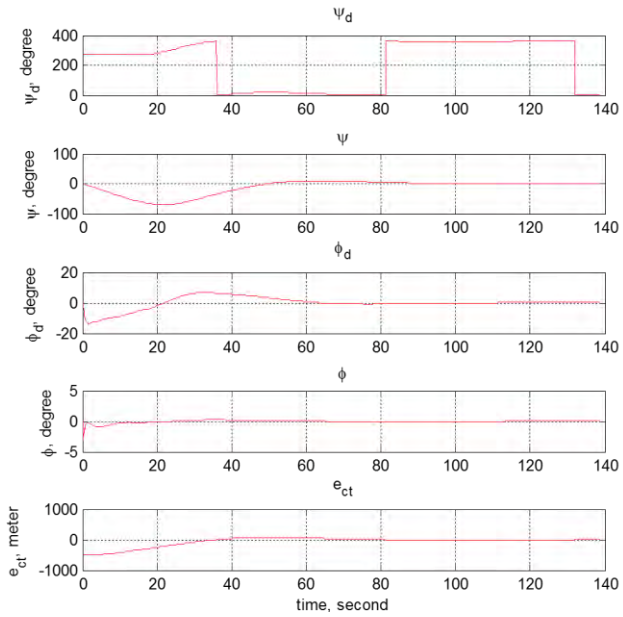

Figure 7. ψ_d: reference heading angle, ψ: measured heading angle, ϕ_d: reference roll angle, ϕ: measured roll angle, e_{ct}: cross track error.

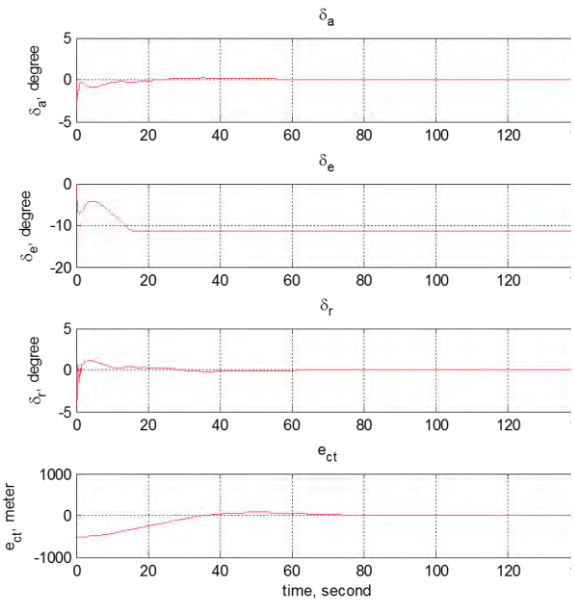

Figure 8. δ_a: aileron deflection, δ_e: elevator deflection, δ_r: rudder deflection, e_{ct}: cross track error.

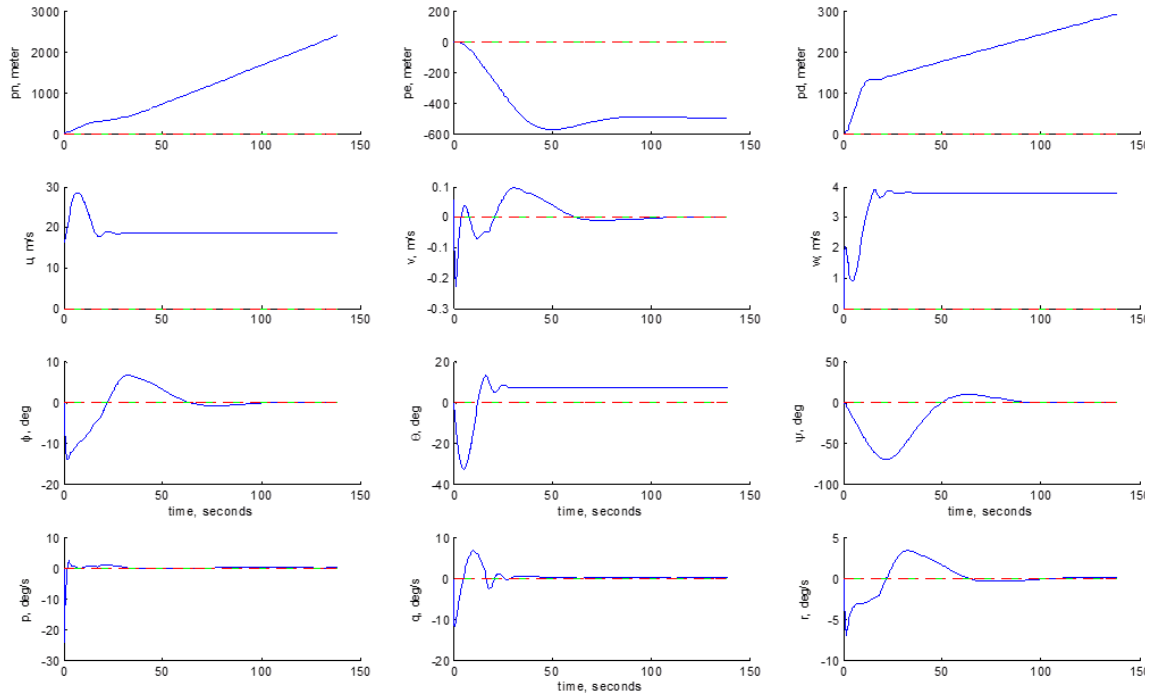

Figure 9. 12 state varibales during simulation. P_n: north position (m), P_e: east position (m), P_d: altitude (m), u: xbody-axis velocity (m/s), v: ybody-axis velocity (m/s), w: zbody-axis velocity (m/s), ϕ: roll angle (degree), θ: pitch angle (degree), ψ: heading angle (degree), p: roll angular rate (deg/s), q: pitch angular rate (deg/s), r: yaw angular rate (deg/s).

5. CONCLUSION

In this study, an unmanned aerial vehicle is made to converge to a predefined path with the help of developed virtual target chasing algorithm. For turning maneuvers, the coordinated turn relations have been considered to calculate the roll angle and turning velocity. A specific reference roll angle is defined according to the difference between the reference heading and the current heading angles. According to the reference roll angle and the true airspeed of the airplane, a reference yaw rate and pitch rate have been calculated.

During the simulation, it is observed that at the very beginning of the simulation there occurs some kind of fluctuation, which is considered as the small difference between the initial conditions and the trim values. After reaching the equilibrium condition, the airplane first flies to the closest point on the path, and as getting closer to the path, it starts to maneuver and follows the path. Although there is an altitude loss until the plane reaches the equilibrium point, the loss of altitude is negligible in the subsequent movements. For the coordinated turn approximation, the thrust ratio also must be auto controlled to sustain the airspeed and altitude. In the simulations, the thrust ratio remains as a constant value. Although a small altitude loss occurred, this did not affect the flight condition dramatically. The aircraft is made to hold the desired pitch rate and yaw rate coming from the coordinated turn relations.

In this study, a 2-D scenario has been investigated. In the future studies, 3D scenarios will be evaluated, and the trajectory path tracking method will be revised accordingly. Constant altitude approach was made in the control of the pitching motion. This does not contradict the definition of coordination, but in the course of time, sideslip effects will be examined. The developed path tracking algorithms are planned to be tested on a small scale model aircraft by using a flight control card to be designed.

6. REFERENCES

[1] P. B. Sujit, S. Saripalli and J. B. Sousa, "Unmanned Aerial Vehicle Path Following: A Survey and Analysis of Algorithms for Fixed-Wing Unmanned Aerial Vehicless," in *IEEE Control Systems*, Vol. 34, No. 1, pp. 42-59, 2014.

[2] V. Cichella, E. Xargay, V. Dobrokhodov, I. Kaminer, A. M. Pascoal, and N. Hovakimyan, "Geometric 3D path-following control for a fixed-wing UAV on SO(3)," in *Proceedings AIAA Conf. Guidance, Navigation Control*, 2011, pp. 3578–3592.

[3] D. R. Nelson, D. B. Barber, T. W. McLain and R. W. Beard, "Vector Field Path Following for Miniature Air Vehicles," in *IEEE Transactions on Robotics*, Vol. 23, No. 3, pp. 519-529, 2007.

[4] L. E. Dubins, "On curves of minimal length with a constraint on average curvature and with prescribed initial and terminal positions and tangents," *American Journal of Mathematics*, Vol. 79, No. 3, pp. 497–516, 1957.

[5] Steven M. LaValle, "Planning Algorithms," University of Illinois, sf. 732, 2006.

[6] J. H. Blakelock, *Automatic Control Aircraft and Missiles*. New York: John Wiley and Sons, 2nd ed., 1991.

[7] R. Rysdyk, "Course and Heading Changes in Significant Wind," *Journal of Guidance, Control, and Dynamics*, Vol. 30, No. 4, pp. 1168-1171.

[8] B. Etkin, *Dynamics of Atmospheric Flight*, New York: Wiley, 1972, pp. 423

[9] R. W. Beard, T. W. McLain, "Small Unmanned Aircraft: Theory and Practice," New Jersey: Princeton Uni., sf. 276, 2012.

[10] J. Roskam, *Airplane Flight Dynamics and Automatic Flight Controls Part I*, Kansas: Design, Analysis and Research Corporation, 2011, Chap. 4.

[11] Z. Öznalbant, M.Ş. Kavsaoğlu, "Design and Flight Test Study of a VTOL UAV," 53rd AIAA Aerospace Sciences Meeting, 5-9 January 2015, Kissimmee, Florida

[12] U. Özdemir, M.Ş. Kavsaoğlu, "Simulation and Control of Fixed Wing Aircraft after a Major Component Loss," 48th AIAA Aerospace Sciences Meeting Including the New Horizons Forum and Aerospace Exposition, 4 - 7 January 2010, Orlando, Florida

VITAE

Zafer Öznalbant

Dr. Zafer Öznalbant graduated from Aeronautical Engineering Department of Aeronautics and Astronautics Faculty of Istanbul Technical University in 2005. He received his M. Sc. degree from the same department under the supervision of Prof. Dr. Mehmet Ş. Kavsaoğlu in 2008 and Ph. D. degree from Anadolu University Faculty of Aeronautics and Astronautics under the supervision of Prof. Dr. Mehmet Ş. Kavsaoğlu and Prof. Dr. Mustafa Cavcar in 2016. His principle research of interests are Flight Mechanics, Unmanned Aerial Vehicles and Path Following. He currently works as a senior flight control system engineer in Turkish Aerospace Industries, Inc.

Uğur Özdemir

He currently works as an Assist. Prof. at Anadolu University. He has received B.S., M.Sc. and Ph. D. degrees in the area of aeronautical engineering from Istanbul Technical University. His research interests are flight dynamics & control, and aircraft design.

Mehmet Şerif Kavsaoğlu

He received his B.S. and M.Sc. degrees from Istanbul Technical University. He completed the von Karman Institute for Fluid Dynamics Diploma Course and he received his Ph. D. degree from Virginia Polytechnic Institute and State University. He served as a faculty member at Middle East Technical University and Istanbul Technical University. Currently, he is a faculty member at the Faculty of Aeronautics and Astronautics, Anadolu University. His research and teaching areas are aerodynamics, aircraft design and flight mechanics.